

Iron orbital occupancies upon valence mixing of charge-ordered $\text{GdBaFe}^{\text{II}}\text{Fe}^{\text{III}}\text{O}_5$

J. Lindén · F. Lindroos · P. Karen

© Springer Science+Business Media Dordrecht 2013

Abstract Mössbauer spectra of charge-ordered/valence-mixed $\text{GdBaFe}_2\text{O}_5$ have been analyzed in order to determine the orbital occupancies of the minority-spin d electron as a function of temperature. In the charge-ordered state below the Verwey temperature T_V , it occupies the Fe^{2+} d_{xz} orbital, which is ordered. Above T_V , the electron partially occurs also at the trivalent iron and spreads over two additional orbitals, $d_{x^2-y^2}$ and d_{z^2} . In the valence-mixing state (above T_p) also orbital d_{yz} participates. The study illustrates how the Mössbauer electric-field gradient, center shift and internal field jointly reflect the distribution of the minority-spin electron culprit behind the Verwey transition.

Keywords ^{57}Fe Mössbauer spectroscopy · Charge ordering · Valence mixing · Mixed valence · Double perovskites

1 Introduction

The antiferromagnetic A-site ordered perovskite $R\text{BaFe}_2\text{O}_5$ (R is a rare-earth element) contains Fe^{2+} and Fe^{3+} that order at low temperatures and mix at high temperatures [1]. The valence mixing proceeds in two steps [2], where the first one, at the lower transition temperature T_V , has all features of the Verwey transition [3] in magnetite. Above the second transition temperature T_p , iron is in a single valence state $\text{Fe}^{2.5+}$. At low temperatures, a long-range order of alternating chains of di- and trivalent iron coordinations along b (Fig. 1) is observed by neutron- [2] and synchrotron X-ray powder diffraction [4].

Proceedings of the 32nd International Conference on the Applications of the Mössbauer Effect (ICAME 2013) held in Opatija, Croatia, 1–6 September 2013

J. Lindén (✉) · F. Lindroos
Physics Department, Åbo Akademi University, 20500 Turku, Finland
e-mail: jlinden@abo.fi

P. Karen
Department of Chemistry, University of Oslo, 0315 Oslo, Norway

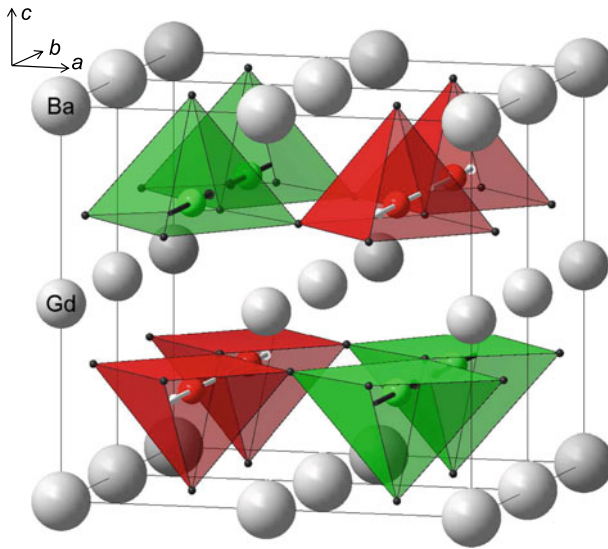


Fig. 1 The magnetic unit cell of charge-ordered $\text{GdBaFe}_2\text{O}_5$ is the same as for $\text{TbBaFe}_2\text{O}_5$ [2]

Mössbauer spectroscopy detects also the short-range order. Upon heating through T_V , the hyperfine parameters change abruptly, and at T_p precipitously [6], with continuous evolution in between [1, 2, 7–9]. Because these changes are mainly associated with the minority-spin d -electron of Fe [8–10], it is possible to calculate its orbital populations from the hyperfine data. Previously this has been done for the two end members $R = \text{Nd}, \text{Pr}$ of this series, which, however, do not exhibit a full unit-charge separation in the charge-ordered state below T_V [9]. Here we report the results of similar calculations for $\text{GdBaFe}_2\text{O}_5$ of a higher iron charge separation.

2 Experimental

Synthesis Single-phase $\text{GdBaFe}_2\text{O}_{5.010}$ and $\text{GdBaFe}_2\text{O}_{5.019}$ were synthesized as described in Ref. [4]. As shown in Ref. [5], thermal parameters of the valence-mixing transitions are practically the same within this oxygen non-stoichiometry range.

Mössbauer measurements ^{57}Fe Mössbauer spectra were recorded in transmission geometry with a less than year-old 25 mCi $^{57}\text{Co:Rh}$ (Cyclotron Co) source kept at room temperature. The absorber temperatures between 77 and 325 K were maintained by an Oxford CF506 continuous-flow cryostat operating with liquid N_2 . Temperatures between 300 and 450 K were controlled by a home-built resistive heater with the sample placed in a dry N_2 atmosphere.

The spectra obtained below the Néel temperature T_N were fitted with a full Hamiltonian of combined electric and magnetic interactions as described previously [8]. The fit parameters were the component intensity I , line width Γ (constrained equal for all components), internal field B and its width ΔB of a gaussian distribution, quadrupole-coupling constant eQV_{zz} , asymmetry parameter η (fixed to zero for all except charge-ordered components),

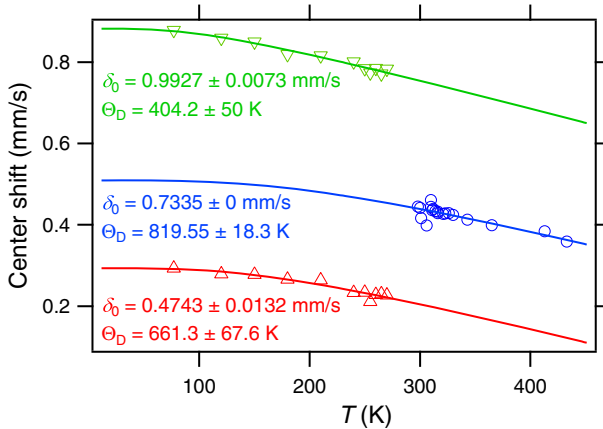


Fig. 2 Parameters for correction on second-order Doppler shift according to fit with (1) for Fe²⁺ (∇), Fe³⁺ (Δ) and Fe^{2.5+} (○)

center shift δ , and the angle β between B and eQV_{zz} set to either 0 or 90° due to ambiguity between the angle turning by 90° and the sign inversion of V_{zz} .

Analysis of the hyperfine parameters Before investigating the influence of the d -electron concentration on the hyperfine fields, their intrinsic temperature dependences had to be compensated for. The center shift $\delta(T)$ consists of isomer shift δ_0 and the temperature-dependent second-order Doppler shift [11]:

$$\delta(T) = \delta_0 - \frac{9k_B\Theta_D}{16Mc} - \frac{9k_B T}{2Mc} \left(\frac{T}{\Theta_D}\right)^3 \int_0^{\frac{\Theta_D}{T}} \frac{x^3 dx}{e^x - 1}, \tag{1}$$

where c is the velocity of light, Θ_D the Debye temperature, k_B the Boltzmann constant, M the mass of the ⁵⁷Fe atom, and T temperature. Least-squares fit with (1) of the center shifts in the temperature range of the charge-ordered phase yield δ_0 and Θ_D for Fe²⁺ and Fe³⁺ (Fig. 2). For the valence-mixed component, δ_0 was fixed to the average of Fe²⁺ and Fe³⁺ (when not fixed, the less precise δ_0 is larger by 0.0121 mm/s than the used average).

A mean-field model is used for the thermal decay of the ordered spin. The magnetic field seen by the Mössbauer nucleus decreases from B^0 at 0 K to zero at T_N . The standard temperature dependences for the integer and semi-integer iron valences were obtained by fitting their $B(T)$ to the following parametric function [12]:

$$\frac{B(T)}{B^0} = \text{Brill}(J, \zeta) = \frac{T}{T_N} \frac{J + 1}{3J} \zeta, \tag{2}$$

where $\text{Brill}(J, \zeta)$ is the Brillouin function:

$$\text{Brill}(J, \zeta) = \left(1 + \frac{1}{2J}\right) \coth \left[\left(1 + \frac{1}{2J}\right) \zeta \right] - \frac{1}{2J} \coth \left(\frac{1}{2J} \zeta \right), \tag{3}$$

in which ζ is a ratio of magnetic and thermal energies and J is the total angular-momentum quantum number. The fits for the standard valences, with B^0 , J and T_N as parameters, are shown in Fig. 3. With these parameters, B^0 for each temperature in the intermittent range of mixed valences was calculated from $B(T)$ via ζ from (2) plugged into (3), with subsequent

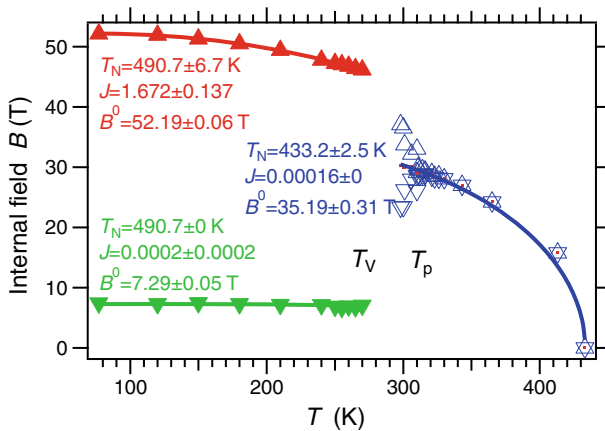


Fig. 3 Parameters for correction on thermal decay of the internal field B according to fit with (2) for Fe^{2+} (∇), Fe^{3+} (Δ) and $\text{Fe}^{2.5+}$ (\bullet)

weighting of the two obtained B^0 into the average corresponding to the component's valence at the given temperature.

Table 1 Valence contributions to EFG and to dipolar field B_{dip} from one minority-spin electron of spin along b ($\equiv y, z \parallel c$ of the crystal). Ligand contributions to EFG

(5):	d_{xy}	d_{xz}	d_{yz}	$d_{x^2-y^2}$	d_{z^2}	$\text{Fe}_{\text{ligand}}^{2+}$	$\text{Fe}_{\text{ligand}}^{3+}$	$\text{Fe}_{\text{ligand}}^{2.5+}$
	n_3	(n_4)	n_1	n_2				
$B_{\text{dip}} \parallel y$ (T)	-17	34	-17	-17	17	-	-	-
eQV_{xx} (mm/s)	-2.4	-2.4	4.8	-2.4	2.4	-0.25	-0.35	-0.52
eQV_{yy} (mm/s)	-2.4	4.8	-2.4	-2.4	2.4	-0.97	-0.35	-0.58
eQV_{zz} (mm/s)	4.8	-2.4	-2.4	4.8	-4.8	1.22	0.70	1.10

Three sources contributing to the temperature-corrected internal field B^0 were considered in this study:

$$B^0 = B_{\text{FC}} + B_{\text{dip}} + B_L, \tag{4}$$

where B_{FC} is the Fermi-contact field proportional to the electron spin, B_{dip} the dipolar field of the valence electrons and B_L the orbital field. B^0 is usually dominated by B_{FC} . A magnetic dipolar field may contribute for all valence electron configurations except high-spin d^5 . The 6th (minority-spin) electron of Fe^{2+} is therefore behind dipolar fields in all our spectra. The dipolar fields for the individual d orbitals occupied by one minority-spin electron of spin along b are listed in Table 1, as estimated in Ref. [9]. The sum of these contributions is zero, and likewise so for all three t_{2g} orbitals: d_{xy} , d_{xz} and d_{yz} and for the two e_g orbitals $d_{x^2-y^2}$ and d_{z^2} .

The electric-field gradient (EFG), of which V_{zz} is the main component, has a very weak intrinsic temperature dependence due to thermal expansion or changes in the phonon spectra [13], which is neglected in this work beyond two structure snapshots at 100 and 300 K

of the charge-ordered and valence-mixed phases, respectively [7]. The temperature-induced changes to V_{zz} are almost exclusively due to changes in the d -electron population. Two sources of EFG were considered: the valence-electron contribution from the minority-spin electron and the ligand contribution from the five oxygen ions of point-charge estimated in Ref. [8, 9]. Also the valence contribution has been estimated previously [9] for one minority-spin electron in alternatively each of the five orbitals, as listed in Table 1 together with the estimated ligand contributions. Like for the dipolar fields, the sum of all valence contributions of one minority-spin electron is zero for t_{2g} and e_g orbitals and their sum.

With n_1 , n_2 and n_3 denoting the populations of the minority-spin electron in $d_{x^2-y^2}$, d_{z^2} and d_{xz} , respectively, the following five equations are constructed from values in Table 1:

$$n_1 + n_2 + n_3 = p \quad (5a)$$

$$-17n_1 + 17n_2 + 34n_3 - B_{FC} \frac{5-p}{5} + pB_L = -B^0 \quad (5b)$$

$$-2.4n_1 + 2.4n_2 - 2.4n_3 + eQV_{xx}^{\text{ligand}} = eQV_{xx} \quad (5c)$$

$$-2.4n_1 + 2.4n_2 + 4.8n_3 + eQV_{yy}^{\text{ligand}} = eQV_{yy} \quad (5d)$$

$$4.8n_1 - 4.8n_2 - 2.4n_3 + eQV_{zz}^{\text{ligand}} = eQV_{zz} \quad (5e)$$

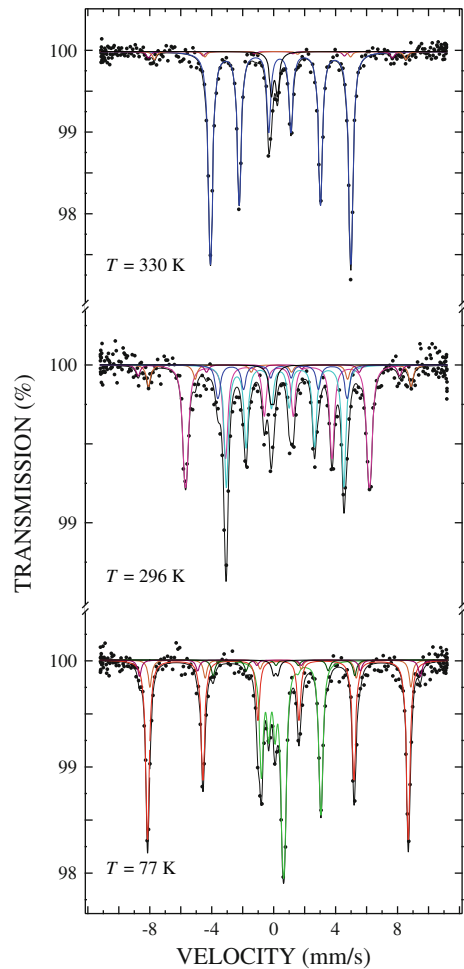
where $0 \leq p \leq 1$ is the total minority-spin population determined from the iron valence of the Mössbauer component, V_{xx} and V_{yy} can be determined from the measured V_{zz} and η by combining the Laplace's equation $\nabla^2 V = 0$ with the asymmetry parameter $\eta = \frac{|V_{xx} - V_{yy}|}{|V_{zz}|}$, B_L is the orbital field corresponding to the angular momentum the iron Mössbauer component can carry per unit of the minority-spin electron as estimated below. Only three of the five (5) are needed, hence the rows (5a) and (5b) are combined with either (5c) or (5e) depending on direction of V_{zz} . When V_{zz} is parallel to b , like for charge-ordered Fe²⁺, the rows (5b) and (5d) are linearly dependent. If so, η and V_{zz} are used to calculate V_{xx} or V_{yy} so that the row (5c) or (5e) can be used. A rational solution of the set of (5) is obtained when all resulting populations are non-negative within reasonable accuracy, and $|V_{zz}| \geq |V_{yy}| \geq |V_{xx}|$ is valid for all EFG components.

The presence of an orbital field B_L depends on whether the expectation value for the angular momentum operator is non-zero. Its component L_y (along b) is non-zero for a wave function ψ of $d_{x^2-y^2}$, d_{z^2} and d_{xz} when proper phase angles are introduced [9]. Other components of B_L are then exactly zero for this combination of wave functions, as the expectation values of L_x and L_z are zero. The phase angles will not affect other hyperfine parameters because the latter depend only on spin- or charge densities, which in turn are proportional to phase-independent probability density $\psi\psi^*$ of the wave function. The spin-orbit interaction always maximizes the orbital field for a non-zero expectation value of L_y . When expressed per number of minority-spin electrons, the maximum is:

$$|B_L| = \frac{2B_L^0}{p_c} \left[\sqrt{n_{1c}n_{3c}} + \sqrt{3n_{2c}n_{3c}} \right] \quad (6)$$

where B_L^0 is a constant that converts the angular momentum to the orbital field at the Fe nucleus [9]. The partial and total populations of the d -orbitals n_{1c} , n_{2c} , n_{3c} and p_c have a subscript "c" to indicate that the minority-spin electron carrying the orbital field is shared between two adjacent Fe sites due to valence-mixing and will therefore conserve this value whereupon it is the smaller of the two that controls the actual field housed by the two sites. In practice, B_L was calculated for both Fe Mössbauer components, and the smaller was always chosen. As B_L depends on the population numbers, (5) has to be solved iteratively,

Fig. 4 ^{57}Fe Mössbauer spectra of $\text{GdBaFe}_2\text{O}_{5.010}$ as a charge-ordered (77 K), partially valence-mixed (296 K) and valence-mixed (330 K) phase. The main components of di- and trivalent parentage are drawn in green and red, the intermittent components in cyan and magenta, respectively. The valence-mixed components are blue. A paramagnetic defect is drawn in black. Trivalent defect components are in brown and purple



yielding $B_L^0 = 10.0$ T, and this value is also used in the present study upon assumption that it reflects a general property of the iron d orbitals.

3 Results and discussion

Mössbauer spectra of the three mixed-valence phases of $\text{GdBaFe}_2\text{O}_{5.010}$ are shown in Fig. 4. The spectrum of the charge-ordered phase that occurs below $T_V \approx 270$ K [7], is dominated by a ~ 50 tesla component of high-spin Fe^{3+} and a ~ 7.5 tesla component of high-spin Fe^{2+} . The unusually small field of the latter is due to the strong counteracting dipolar field of the minority-spin electron occupying the d_{xz} orbital (Table 1). Upon heating through T_V , increasing amount of this minority-spin electron is abruptly transferred to the originally trivalent Fe, decreasing its internal field and increasing the field of the originally divalent component. After that, a continuous evolution leads to a precipitous change at T_p in favor of

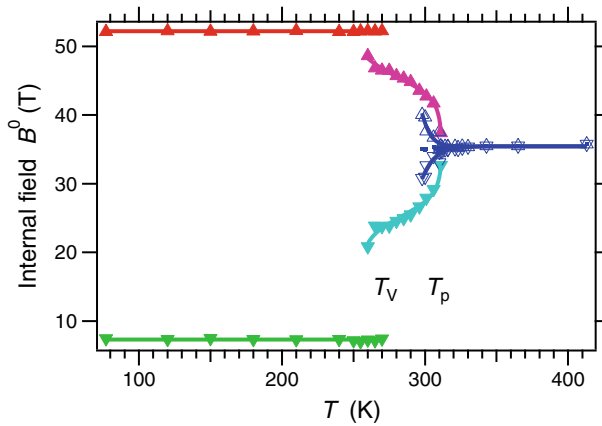


Fig. 5 Temperature evolution of B^0 that reflects the pure effect of the gradual valence mixing. Fit functions: average for charge-ordered components, sigmoid for valence-mixed and inverse sigmoid for intermittent components

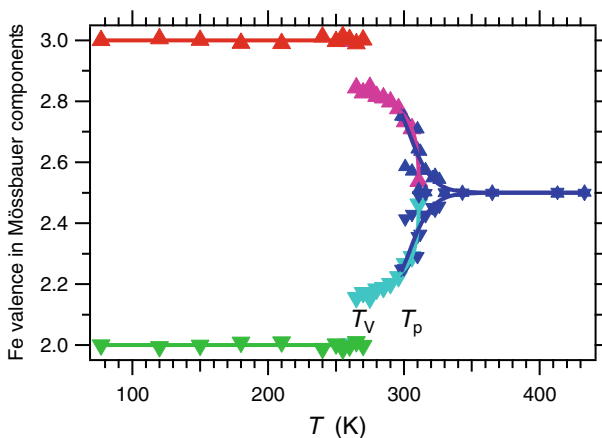


Fig. 6 Temperature evolution of iron valence for the main components of di- and trivalent parentage (∇ , Δ , respectively): charge ordered (green and red), intermittent (cyan and magenta) and valence mixed (blue). Fit functions: average for charge-ordered components, sigmoid for valence-mixed and inverse sigmoid for intermittent components

the twin valence-mixed components that become indistinguishable around 330 K. The temperature evolution of the internal field in Fig. 5 and of the iron valences in Fig. 6 illustrate this clearly.

Above T_N , the Mössbauer spectrum is dominated by a single line of very small quadrupole splitting and of isomer shift compatible with the valence-mixed state +2.5, Fig. 7. A quadrupole-split component of trivalent iron and a very weak magnetic sextet in the background are both attributed to oxidative decomposition at elevated temperatures.

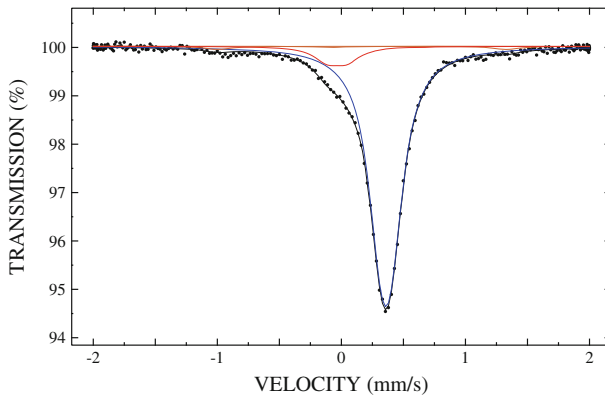


Fig. 7 Paramagnetic Mössbauer spectrum of $\text{GdBaFe}_2\text{O}_{5.019}$ at 433 K. Components due to valence-mixed Fe (blue unresolved doublet), trivalent Fe (red doublet) and a weak magnetic sextet (brown) were discerned

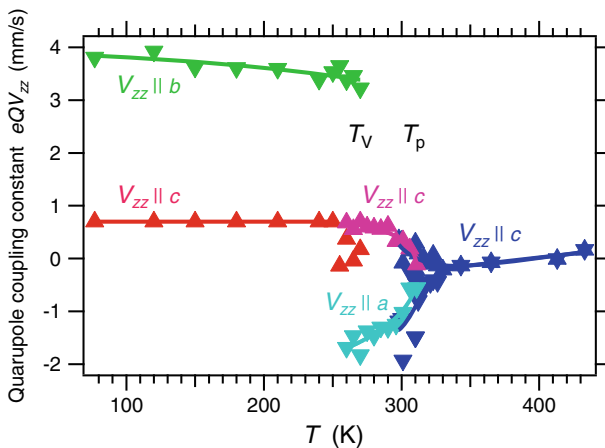


Fig. 8 Temperature evolution of eQV_{zz} for the three groups of main iron components of di- and trivalent parentage (∇ , Δ , respectively): charge ordered (green and red), intermittent (cyan and magenta) and valence mixed (blue). Fit functions: constant for charge-ordered Fe^{3+} , sigmoid for charge-ordered Fe^{2+} , inverse sigmoid for intermittent and sigmoid on a slope for valence-mixed components

3.1 Fitting the spectra

Setting correct direction of V_{zz} is essential for a successful population analysis. Below T_V , the Fe^{2+} component clearly favors $\beta = 0^\circ$, hence $V_{zz}||b$, and also η was readily fitted. The Fe^{3+} component of no orbital contribution to EFG was fitted with β fixed at 90° , hence $V_{zz}||c$ dominated by the ligand contribution (Table 1). The ligand contribution also suggests that $\eta = 0$. However, when η was initially fixed at this value, quadrupole coupling values of only 0.10–0.30 mm/s were obtained. A slight improvement of the fit was achieved by fixing eQV_{zz} at the ligand value of 0.70 mm/s (Table 1) and releasing η .

Above T_V , the fitting attempts were done in parallel with the population analysis. Generally the $\beta = 0^\circ$ option could be ruled out as it produced quadrupole constants too small to

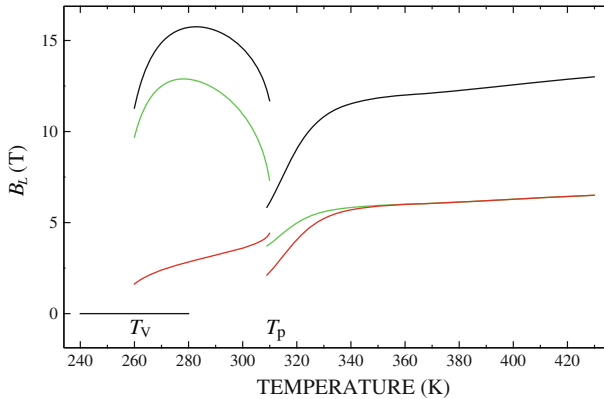


Fig. 9 Estimated orbital field B_L for the minority-spin electron (*black*) separated into contributions from $\text{Fe}^{<2.5+}$ (*green*) and $\text{Fe}^{>2.5+}$ (*red*)

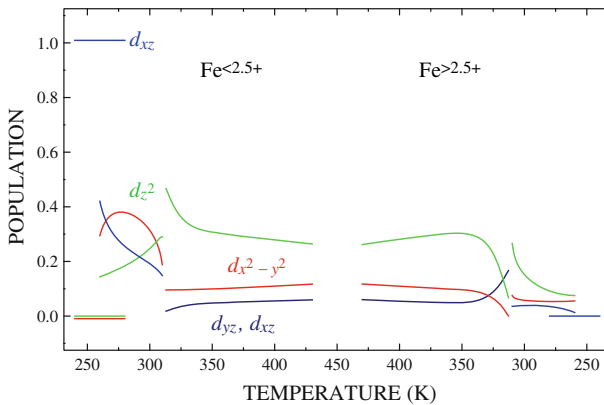


Fig. 10 Temperature evolution of the calculated (5) minority-spin electron populations in the $d_{x^2-y^2}$, d_{z^2} and d_{xz} orbitals of charge-ordered, intermittent and valence-mixed components of di- and trivalent parentage (shown from left and right, respectively) in GdBaFe₂O₅ under thermally induced mixing towards the paramagnetic end point of the fully valence-mixed state. The additional d_{yz} population concerns the valence-mixed components only

be reproduced by (5), suggesting that β should be fixed at 90° . The structural trend towards tetragonality upon heating suggests that $V_{zz}||c$ should be sufficient, which was also the case except for the intermediate Fe component of divalent parentage. The temperature evolution of the quadrupole coupling constants is plotted in Fig. 8.

Fitting the internal field for charge-ordered Fe^{3+} yields $B^0 = 52.19$ T, which in absence of a minority-spin electron is taken as the Fermi-contact field B_{FC} in (5). For all other Fe components, the internal field is influenced by dipolar- and in most cases also orbital contributions.

3.2 Solving the (5)

The temperature evolution of iron valences in Fig. 6 and of hyperfine parameters in Figs. 5 and 8, approximated with suitable functions, were fed point-wise to (5) to obtain the populations and the orbital field B_L . As negative populations and $|V_{zz}|$ smaller than $|V_{xx}|$ or $|V_{yy}|$ cannot be accepted as solutions, the cases of smaller $|V_{zz}|$ in the valence-mixed state were dealt with by introducing a population n_4 of the d_{yz} orbital above T_p . This is justified by the increasing tetragonality that decreases the energy difference of d_{xz} and d_{yz} (Table 1). The introduced 4th variable makes (5) numerically dependent, as the combined contribution of d_{xz} and d_{yz} to the EFG and dipolar field equals that of d_{z^2} . However, considering that two "units" of the minority-spin electron for the combination d_{xz} , d_{yz} have the same effect as one unit of d_{z^2} , a difference arises when about 1/2 minority-spin electron (valence mixing components) is distributed over the orbitals. An initial guess for the d_{yz} concentration was made, the right-hand sides of (5) were adjusted, and populations n_1, n_2, n_3 and B_L solved iteratively. When $|V_{xx}|$ and $|V_{yy}|$ exceeded $|V_{zz}|$, the initial n_4 was updated and the cycle repeated. It should be pointed out that despite introducing a fourth orbital, the (6) still holds as a very good approximation.

The orbital field due to the minority-spin electron and its distribution over the two valences is shown in Fig. 9. In the charge-ordered phase, B_L is zero for Fe^{3+} of no minority spin and zero for Fe^{2+} of one minority-spin electron in d_{xz} that cannot carry an angular momentum (see (6) in which $n_{2c} = n_{1c} = 0, n_{3c} = 1$). The simultaneously determined population numbers are shown in Fig. 10. In the valence-mixed phase, the iterative scheme was constrained to have equal occupancies of d_{xz} and d_{yz} due to tetragonality ($n_4 = n_3$), and this removed the component-size violations within the EFG.

The results in Figs. 9 and 10 reproduce well the observed hyperfine parameters. Only the EFG asymmetry parameter η is modelled poorly. There are several reasons for this: Except for charge-ordered Fe^{2+} , the parameter η cannot be reliably fitted from the spectra. Above T_V , η was fixed at 0 implying $V_{xx} = V_{yy}$, while nothing in the set of (5) ascertains this to be fulfilled, as only p, V_{zz} and B^0 are specified. Furthermore, being a ratio and a difference between EFG components, η is numerically somewhat unstable. Finally, higher-order terms of the EFG from next-neighbor atoms could affect η , despite being too weak to affect V_{zz} significantly.

4 Conclusions

The charge- and orbital order in $\text{GdBaFe}_2\text{O}_5$ is controlled by the single minority-spin electron of divalent iron parentage. At low temperatures, it orders the d_{xz} orbital along rows of Fe^{2+} coordination square-pyramids alternated with Fe^{3+} rows. Above the Verwey transition, the evolution of the hyperfine parameters can be used to extract the temperature-dependent orbital populations of the minority-spin electron. The method should be applicable to Mössbauer spectra of other magnetically ordered phases.

References

1. Lindén, J., Karen, P., Kjekshus, A., Miettinen, J., Pietari, T., Karppinen, M.: *Phys. Rev. B* **60**, 15251 (1999)
2. Karen, P., Woodward, P.M., Lindén, J., Vogt, T., Studer, A., Fischer, P.: *Phys. Rev. B* **64**, 214405 (2001)
3. Verwey, E.J.W.: *Nature* **144**, 327 (1939)
4. Karen, P.: *J. Solid State Chem.* **170**, 9 (2003)
5. Karen, P.: *J. Solid State Chem.* **177**, 281 (2004)
6. Lindén, J., Gustafsson, K., Karen, P.: *J. Solid State Chem.* **180**, 138 (2007)
7. Lindén, J., Karen, P., Yamauchi, H., Karppinen, M.: *Hyp. Int.* **156–157**, 321 (2004)
8. Lindén, J., Karen, P.: *J. Solid State Chem.* **183**, 2703 (2010)
9. Lindén, J., Karen, P.: *Phys. J. Condens. Matter* **24**, 376002 (2012)
10. Spiel, C., Blaha, P., Schwarz, K.: *Phys. Rev. B* **79**, 115123 (2009)
11. Menil, F.: *J. Phys. Chem. Solids* **46**, 763 (1985)
12. Crangle, J.: *Solid State Magnetism*, vol. 24, p. 33. Edward Arnold Publ., London (1991)
13. Torumba, D., Parlinski, K., Rots, M., Cottenier, S.: *Phys. Rev. B* **74**, 144304 (2006)